Abstract

The purpose of this investigation was to examine the fluid dynamic characteristics of the two most commonly used oar blades: the Big Blade and the Macon. Scaled models of each blade, as well as a flat Big Blade were tested in a water flume using a quasi-static method similar to that seen in swimming and kayaking research. Measurement of the normal and tangential blade forces enabled lift and drag forces generated by the oar blades to be calculated over the full range of sweep angles found during a rowing stroke. Lift and drag force coefficients were then calculated and compared between blades. The data revealed that Big Blade and Macon oar blades exhibited very similar characteristics. Hydraulic blade efficiency was not therefore found to be the reason for claims that the Big Blade could elicit a 2% improvement in performance compared to the Macon. The Big Blade was also shown to have similar characteristics to the flat plate when the angle of attack was below 90 degrees, despite significant increases in lift coefficient when the angle of attack increased above 90 degrees. This result suggests that the Big Blade design may not be fully optimised over the whole stroke.

Keywords: Drag, lift, oar blade, rowing

Introduction

To enhance performance in rowing, it is important to maintain a high mean boat velocity (Schneider & Hauser, 1981), requiring a highly efficient stroke. This is achieved by the crew applying large input forces to the oar handle that are transferred to the water by the oar shaft and blade as output forces (Figure 1).

Figure 1 near here

The first oars in rowing were constructed from wood (Herberger, 1987), and the oar blades were of a long, flat and thin "pencil" design (Dudhia, 2000). In the 1950s, crews started experimenting with shorter, wider and curved blades, and in 1958, a German crew used what is now known as the "Macon" blade (Figure 2), named after the venue for the world championships of that year (Sayer, 1996;Pomponi, 1994;Pinkerton, 1992). Blade shape did not change significantly from the Macon shape until 1991 when Concept 2 introduced an asymmetrical blade shape, named the "Big Blade" after its larger surface area (Nolte, 1993;Dreher, 1997;Dreissigacker & Dreissigacker, 2005), with this new design being made possible through the advancement of the understanding of composite materials (Pinkerton, 1992). As was also the case in boat design, composite materials allowed for lighter blades with increased stiffness, therefore improving the efficiency of the blade (Sayer, 1996;Dal Monte & Komor, 1989). Despite the improvements in the construction of oar blades, their fluid dynamic characteristics have yet to be fully explored, with blade designs being based upon trial and error approaches (Pinkerton, 1992).

Figure 2 near here

The sequence of oar blade movements during the stroke that give rise to the propulsion produced by the blade has previously been broken down into four phases (Figure 3). These illustrate the relative magnitudes of propulsive lift and drag forces generated by the oar blade for varying sweep angles (Dreissigacker & Dreissigacker, 2000). The movement of the oar blade relative to the water during these phases will generate both lift and drag forces similar to any aerofoil (Nolte, 1984). Figure 3 shows that for optimal stroke efficiency, high lift forces must be achieved at the start (phases 1 and 2) and end (phase 4) of the stroke, with high drag forces being required as the oar shaft approaches a position perpendicular to the line of the boat (phase 3).

Due to the complex sequence of movements between the oar blade and the water affecting lift and drag, the fluid dynamic characteristics of oar blades must be determined in order to assess the success of any oar blade design. Yet, in spite of the profound effect of hydraulic performance of oar blades on rowing propulsion, few attempts have been made to measure these characteristics (Barre & Kobus, 1998;Ramsey, 1993;Jonker & Yenson, 2002). The studies made used a dynamic approach, which limits the applicability of the data to only the blade movement paths produced by their methods. Due to the complex and variable path of the oar blade in rowing, it is more appropriate to use a quasi-static approach (Toussaint *et al.,* 2002) as used previously in both swimming (Berger *et al.*, 1995) and kayaking (Sumner *et al.*, 2003), which involve either the hand or blade being held static in a water flume at a range of angles similar to those encountered during each stroke, and the resultant fluid force being recorded at each sweep angle. Using this method allows the force characteristics of each oar blade to be applied to any rowing condition unlike the previously discussed dynamics studies (Barre & Kobus, 1998;Ramsey, 1993;Jonker & Yenson, 2002). This force data can then be combined with measured, or modelled, kinematic data to estimate propulsive forces during the stroke. Berger et al. (1999) recently showed there to be only a 5% difference between using measured propulsive force and quasi-static data, with some of this error being due to the error in simulating hand kinematics, which suggests that quasi-static simulations are appropriate and accurate. A limitation of using the quasi-static approach, however, is that forces generated by the development of any non-steady-state vortices about the oar blade are ignored. However, to take account of these dynamic factors, a complex computational fluid dynamic model would be required, which was beyond the scope of the present investigation.

Figure 3 near here

The purpose of the present investigation was, therefore, to determine the fluid dynamic characteristics of the Big Blade and Macon oar blade designs in order to assess their ability to successfully generate lift and drag forces during the rowing stroke. It was expected that the Big Blade would show an improved ability to generate fluid forces when compared to the Macon in line with the performance advantage claimed by the manufacturers, and that blade curvature would also have a positive influence on the fluid forces generated.

Methods

Oar blades

The fluid dynamic tests were performed in a water flume which had a free stream width and depth of 0.64m and 0.15m, respectively. Due to the inherent edge resistance effects on the free stream velocity, it was decided that quarter scale oar blade models should be used so that the length of the blades were less than a quarter of the flume width and remained in the part of the flume where velocity reductions were minimal. The model blades were fabricated from 1.8mm thickness aluminium sheet, which was shown by dimensional analysis to provide sufficient stiffness to be able to discount any influence of oar blade bending. Although this model thickness transfers to a blade thickness of 7.2mm, compared to the full size oar blade thickness of 5mm, a model thickness of 1.8mm was required to avoid any influence of blade flexing. Compared to the influence the shape of the blade, this increase in blade thickness is unlikely to have a significant influence of blade characteristics. A number of oar blade designs were tested including the Macon and Big Blade designs (Concept 2, Morrisville, USA), and a flat plate with the same shape and projected area as the Big Blade. Both the Big Blade and Macon oar blade designs have both longitudinal and lateral curvature. However, due to manufacturing limitations, only the longitudinal curvature could be modelled. Traditionally, both oar blade designs have a spine which runs along the line of the oar shaft and extend approximately half way along the length of the blade. However, recent advances in oar blade design have seen the removal of this spine from the face of the blade (e.g. Big Blade Smoothie, Concept 2, Morrisville, USA). Therefore the model blades used in the present investigation were manufactured without a spine. The flat plate was tested in order to determine the influence of blade curvature.

Experimental setup

In order to measure the forces being applied to the oar blade models, a measurement system was designed such that the model blades could be held static in the flume at a range of angles relative to the direction of free stream. The blades were attached to a model oar shaft, with their normal orientations relative to the shaft (Figure 2), and the model shaft made an angle of 10 degrees with the water surface. This model oar shaft was attached to a vertical bar, and strain gauges were located on both the oar shaft and vertical bar in order to record the normal and tangential fluid forces generated by the model oar blades (Figure 4).

<u>Figure 4 near here</u>

This allowed for the determination of lift and drag forces using the equations,

$$F_{Lift} = F_T \sin\alpha + F_N \cos\alpha \quad (1)$$

and

$$F_{Drag} = F_N \sin\alpha - F_T \cos\alpha \quad (2)$$

where F_T is the blade force acting tangentially to the blade chord line (Figure 5), F_N is the blade force acting normally to the blade chord line and α is the angle of attack between the blade chord line and the free stream direction of fluid flow (Figure 5). The angular position of the vertical bar in the horizontal plane, and hence the angle α of the oar shaft, was measured using a 360 degree smart position sensor (601-1045, Vishay Spectrol, UK), which had a stated linearity of ±1 % and a resolution of 0.5 degrees. This position sensor was powered by a fixed voltage power supply (5 volts), and the output of the position sensor was displayed on a digital volt meter. For a detailed description of the design and calibration of the measurement system, and the reduction of lift and drag forces from the strain gauge recordings, see Caplan and Gardner (2005).

Figure 5 near here

Lift force, F_L, and drag force, F_D, of an oar blade can be modelled by the relationships,

$$F_L = \frac{1}{2} C_L \rho A V^2 \qquad (3)$$

and

$$F_D = \frac{1}{2} C_D \rho A V^2 \qquad (4)$$

where ρ is the fluid density, A is the projected area of the oar blade measured perpendicularly to the face of the blade, and V is the relative velocity between the oar blade and water (Munson *et al.*, 2002). C_L and C_D are dimensionless force coefficients which are dependent upon the oar blade shape and the angle of attack between oar blade chord line and fluid flow direction. In order to compare the fluid dynamic characteristics of oar blade designs, it is appropriate to calculate and compare the force coefficients in order to discount any influence of fluid velocity, fluid density, and projected area.

Experimental protocol

Before each blade was tested, reference flow conditions were established by making a point velocity measurement at a depth of 25mm from the water surface in the centre of the flume using a miniature current flowmeter probe (403, Nixon, UK), and the rotational frequency of the probe was displayed on a flow meter (Streamflo 400, Nixon, UK).

A ten second base line force measurement was taken and the data averaged over the duration of this period. The oar blade was then placed in the flume so that the blade chord line was in line with the direction of free stream (α = 0 degrees), and with the top edge of the blade flush with the water surface. Signals from the strain gauges passed through a custom made strain gauge amplifier before passing to an analogue-digital card (PC-DAS 16/12, Measurement Computing, USA), which sampled the data at a frequency of 2.5 kHz for a period of 15 seconds for each trial. Four 15 second trials were collected at each angle of attack.

The angle of attack was increased in 5 degrees intervals between 0 – 180 degrees. The data collected during each 15 second collection period was averaged to provide four mean voltages for each strain gauge bridge at each angle. These voltages allowed for the calculation of lift and drag forces as described earlier and in Caplan and Gardner (2005). The water temperature was measured at 16 degrees, which equated to a fluid density of 999 kg.m^3. This value, along with the projected areas of the oar blades given in Table 1, the measured fluid velocity and lift and drag forces were substituted into equations (1) and (2) to provide lift and drag coefficients for each angle of attack tested. A macro image analyser (Carl Zeiss, Germany), was used to photograph the blades from directly above and the software Axio Vision (Carl Zeiss, Germany), was subsequently used to determine the projected area of each blade image shown in Table 1.

Table 1. Projected areas for the model oar blades tested.

Blade Description	**Projected Area (cm^2)**
Flat plate	77.42
Big Blade	77.41
Macon	67.48

Influence of Reynolds number

As with any fluid dynamic test involving the use of scaled models, both geometric (aspect ratio) and dynamic (Reynolds number) similarity must be achieved in order for the model data to be directly applied to the real life situation. As the models were scaled exactly from the full size oar blades, geometric similarity was met. However, due to the scale of the models and the maximum velocity that could be achieved by the water flume, it was not possible to gain Reynolds number similarity. It was therefore necessary to determine the Reynolds number dependence of the lift and drag coefficients. Reynolds number is given by

$$\mathrm{Re} = \frac{\rho V l}{\mu} \tag{5}$$

where ρ is the fluid density, V is the fluid velocity, l is a characteristic length of the object, and μ is the kinematic viscosity of the fluid (Munson *et al.*, 2002). The dependence of the model data on Reynolds number can therefore be determined by varying either the model size or relative free stream velocity. Due to the edge effects of the water flume, with the fluid velocity reducing as the edges are approached, the measured force coefficients would be influenced by a reduced average free stream velocity across the frontal area of the blade if the blade size was increased. Therefore, the flat plate, the simplest of blade designs, was tested at a range of fluid velocities, between 0.4 - 0.85 $m.s^{-1}$ using the protocol described above. It was found that lift and drag coefficients were independent of Reynolds number with a free stream velocity above 0.7$m.s^{-1}$, as discussed in the next section. A fluid velocity of 0.75 ms^{-1} was therefore used for the remainder of the tests, which was high enough to overcome any influence of Reynolds number, but not so high that the increasing turbulence of the water interfered with the measurement system.

Data analysis

The calculated lift and drag coefficients were compared between oar blade designs. Independent samples t-tests were used at each angle, α, to determine if the difference between oar blade designs was significant at each angle tested, with a 99% confidence level ($p<0.01$) being used throughout.

Results and discussion

The simplest of oar blade designs was the flat plate with the same perimeter shape and projected area as the Big Blade. Figure 6 shows both drag and lift coefficients for this oar blade plotted against angle of attack. An angle of attack less than 90 degrees indicated that the leading edge of the oar blade was the tip of the blade, with an angle of attack greater than 90 degrees indicating that the leading edge had changed to the shaft end of the oar blade.

Drag coefficient (C_D) was seen to increase with angle of attack until an angle close to 90 degrees was reached, at which point the maximum (C_{Dmax}) was approximately 2. As the angle of attack increased further, C_D reduced towards zero.

Lift coefficient (C_L) increased with angle of attack until a maximum (C_{Lmax}) was reached at approximately 40-45 degrees, and reduced to zero at 90 degrees. As the angle of attack continued to increase, with the leading edge having changed to the shaft end of the blade, C_L, decreased to a minimum (C_{Lmin}) at approximately 135 degrees. As the angle of attack increased further, C_L increased to zero. Although C_L was negative at angles of attack greater than 90 degrees, the negative sign simply indicated that the direction of the lift force generated by the oar blade changed direction by 180 degrees.

Figure 6 near here

In order to determine the influence of Reynolds number on the measured data, C_{Dmax}, C_{Lmax} and C_{Lmin} were compared for the flat plate presented in Figure 6 at a range of free stream velocities. Figure 7 shows that both C_{Lmax} and C_{Lmin} were virtually unaffected by velocity, and that C_D is independent of velocity above $0.7ms^{-1}$.

<u>Figure 7 near here</u>

The data presented in Figure 7 agreed well with previously published data for the forearm in swimming (Berger *et al.*, 1995;Bixler & Riewald, 2002). Berger et al. (1995) showed that, for a prosthetic human forearm and hand that was dragged through a towing tank, C_L and C_D were only slightly dependent on velocity at free stream velocities above $0.7ms^{-1}$, where the Reynolds number (Re) at this velocity was 6.29×10^4. Bixler and Riewald (2002) used a computational fluid dynamic (CFD) model to predict the flow about a similar hand and forearm model and it was predicted that the coefficients were independent of velocity above $1ms^{-1}$, where Re equalled 9.96×10^4. For the flat plate tested here, Re at $0.7ms^{-1}$ was 9.44×10^4, which was within previously published ranges for Re independence, as discussed above.

Figure 8 looks at the effect of adding longitudinal curvature to the Big Blade design. It was expected that curvature would increase the magnitude of fluid circulation about the blade, thus increasing lift (Batchelor, 2000). At angles of attack below 90 degrees, however, C_L is similar for both the flat and curved blades. This result suggests that some mechanism must play a part in the changes in C_L seen with curvature which negates the increase in lift expected through added circulation. Although increasing the curvature of the blade should, theoretically, increase the fluid circulation around the blade and therefore increase lift, fluid will also separate away from the back of the blade more easily, increasing the turbulence in the boundary layer of the blade, and reducing lift and increasing drag. For maximum lift, the boundary layer flow should be laminar and not turbulent. Hoerner & Borst (1985) show that for low aspect ratio wings, such as the oar blades investigated here, where the aspect ratio (width/height, where height is the longitudinal length relative to free stream direction in this case) is less than 3, the lateral edges, or upper and lower edges for oar blades, play a significant role in the generation of lift. Higher aspect ratio wings simply have a linear increase in lift coefficient with increases in angle of attack (linear lift component), and will typically stall, or reduce its ability to generate lift force, at an angle of attack between 10-15 degrees. This linear component of lift is generated by the longitudinal circulation of the boundary layer fluid particles about the blade. Low aspect ratio wings, however, have both a linear and non-linear component of lift. This non-linear component is thought to be due to the fluid flowing around the lateral edges of the wing (upper and lower edges of the oar blade), generating vortices along these edges which act to assist the attachment of the boundary layer to the back of the wing. This increases the stall angle of attack to approximately 45 degrees (Hoerner & Borst, 1985). It is therefore important for the magnitude of these lateral edge vortices to be as great as possible to reduce the separation causing this turbulent flow.

<u>Figure 8 near here</u>

Figure 8 shows that the curved Big Blade is able to generate lift more effectively than the flat blade when the shaft end of the blade is acting as the leading edge, with the angle of attack being greater than 90 degrees. For the Big Blade, at these angles of attack, the blade begins to resemble the shape of a delta wing, where the distance between the two edges at any point along its longitudinal axis increases from the leading to the trailing edge. This will result in stronger vortices developing along the upper and lower edges (Hoerner & Borst, 1985), allowing the fluid flow to remain attached to the back of the blade for a longer distance along the blade, resulting in the significant increase in C_L that is observed between 140-180 degrees. The effect of blade curvature on boat propulsion is therefore positive at these angles of attack. At angles of attack below 90 degrees, however, lift is not generated as effectively due to the shape of the upper and lower edges.

C_D was seen to be greater for the curved blade above 85 degrees. This increase as the angle of attack approaches 180 degrees is due to the increased contribution of form drag as a result of the curvature increasing the area of the blade visible to the oncoming fluid at these low and high angles. At approximately 90 degrees, more fluid is trapped on the face of the blade (Bird, 1975) generating increased drag and hence increasing C_D. The effect of blade curvature on boat propulsion is therefore positive at angles of attack above 90 degrees and negative at angles below 90 degrees.

Since the introduction of the Big Blade in 1991, performances have improved suggesting an increase in propulsive efficiency between the Big Blade and the Macon blade designs (Dreissigacker & Dreissigacker, 2000;Pomponi, 1994). However, only small differences in C_L were observed between the two blades (Figure 9). C_L was slightly increased for the Big Blade at most angles of attack, although this increase was only significant at a small number of angles when the magnitude of C_L is small.

According to low aspect ratio wing theory, as aspect ratio increases, C_{Lmax} increases and the angle of attack at which C_{Lmax} occurs decreases. At angles of less than 90 degrees this was seen to occur, with the Big Blade (larger aspect ratio) reaching a higher C_{Lmax} at a slightly reduced angle of attack. This effect is less clear at angles greater than 90 degrees.

C_D is similar between blades at angles of attack up to 50 degrees and above 145 degrees. However, between 55-75 degrees a small decrease in C_D is observed for the Macon, but a more substantial increase in C_D occurs between 75-100 degrees which makes an added positive contribution to propulsion and may contribute to the increased performance claimed for the big blade. This effect is likely to be due to the type of fluid flow separation that is occurring around the stall point for this blade.

Nolte (1993) suggested that the cause of the supposed improvements in propulsive efficiency with the Big Blade were due to the fluid flow across the face of the blade being less disturbed than with the Macon, due to the upper surface of the Big Blade running parallel to the water surface, generating more lift. The current data suggests this hypothesis to be incorrect, and the lack of substantial difference in blade performances may suggest that the two blades perform similarly. However, the Macon blade has a smaller projected area than the Big Blade, and if rowers used Big Blades and Macon blades of the same projected area there may be little difference in performance.

Figure 9 near here

Conclusions

The results of the study indicate that both the Macon and Big Blade designs have similar fluid dynamic properties at most of the angles studied. However, the Big Blade generated significantly greater drag coefficients at angles of attack around 90 degrees.

It was expected that the curved Big Blade would be able to generate significantly greater lift coefficients compared to the flat plate. The results of the study, however, indicated that this was only true when the angle of attack was greater than 90 degrees, when the leading edge changed from being at the tip to the shaft end of the oar blade. This finding was attributed to the shape of the upper and lower edges of the oar blade, causing it to act in a similar way to a delta wing during the second half of the stroke.

The findings of this study would suggest that current oar blade designs are not fully optimised. It should therefore be possible to transfer propulsive force to the water more efficiently throughout the duration of the stroke.

Reference List

Barre, S. & Kobus, J.-M. (1998). New facilities for measurement and modelling of hydrodynamic loads on oar blades. In *The engineering of sport*, ed. Haake, S. J., pp. 251-260. Blackwell Science, Cambridge.

Batchelor, G. K. (2000). *An introduction to fluid dynamics.* Cambridge University Press, Cambridge.

Berger, M. A., de Groot, G., & Hollander, A. P. (1995). Hydrodynamic drag and lift forces on human hand/arm models. *Journal of Biomechanics*, **28**, 125-133.

Berger, M. A., Hollander, A. P., & de Groot, G. (1999). Determining propulsive force in front crawl swimming: a comparison of two methods. *Journal of Sports Sciences*, **17**, 97-105.

Bird, W. J. (1975). The mechanics of sculling. *Chartered Mechanical Engineer*, **22**, 91-94.

Bixler, B. & Riewald, S. (2002). Analysis of a swimmer's hand and arm in steady flow conditions using computational fluid dynamics. *Journal of Biomechanics*, **35**, 713-717.

Caplan, N. & Gardner, T. N. (2005). A new measurement system for the determination of oar blade forces in rowing. In *Proceedings of the XXth IASTED International Symposium on Biomechanics*.

Dal Monte, A. & Komor, A. (1989). Rowing and skulling mechanics. In *Biomechanics of sport*, ed. Vaughan, C. L., pp. 53-120. CRC Press, Inc., Boca Raton, Florida.

Dreher, J. Technology discussion: New blade shapes - part 1. *www.durhamboat.com/blade.htm*. Accessed:8/2/03.

Dreissigacker, D. & Dreissigacker, P. (2000). Oars - Theory and Testing. In *Proceedings of the XXIX FISA Coaches Conference.* Sevilla, Spain.

Dreissigacker, D. and Dreissigacker, P. Dreissigacker Oars. *http://www.concept2.com/05/oars/oars_home.asp*. Accessed:8/2/05.

Dudhia, A. A history of Oxford College rowing. *http://www.atm.ox.ac.uk/rowing/history.html*. Accessed:4/1/05.

Herberger, E. (1987). *Rowing: the GDR textbook of oarsmanship.* Sport Books Publisher, Toronto.

Hoerner, S. F. & Borst, H. V. (1985). *Fluid-dynamic lift*, 2 ed. Hoerner Fluid Dynamics, Albuquerque, New Mexico.

Jonker, K. & Yenson, S. (2002). *Quantitative testing of blade performance.* Massachusetts Institute of Technolgy, B.Sc. Thesis.

Munson, B. R., Young, D. F., & Okiishi, T. H. (2002). *Fundamentals of fluid mechanics*, 4th ed. John Wiley & Sons, Inc., New York.

Nolte, V. (1984). *Die Effektivität des Ruderschlages.* Berlin.

Nolte, V. (1993). Do you need hatchets to chop your water? *American Rowing*, **July/August**, 23-26.

Pinkerton, P. (1992). The Big Blade goes big time. *Australian Rowing*, **September**, 10-11.

Pomponi, R. Innovations in oar technology: transition to a new dominant design. *http://groups.google.com/groups?hl=en&lr=&ie=UTF-8&selm=renata-2012941115460001%40ctpid-mac-13.mit.edu*. Accessed:1/1/05.

Ramsey, W. D. (1993). *Lift and drag characteristics of rotating oar blades.* Massachusetts Institute of Technology, B.Sc Thesis.

Sayer, B. (1996). *Rowing and sculling. The complete manual.* St Edmundsbury Press Ltd., Bury St Edmunds.

Schneider, E. & Hauser, M. (1981). Biomechanical analysis of performance in rowing. In *Biomechanics VII-B*, eds. Morecki, A., Fidelus, K., Kedzior, K., & Wit, A., pp. 430-435. University Park Press, Baltimore.

Sumner, D., Sprigings, E. J., Bugg, J. D., & Heseltine, J. L. (2003). Fluid forces on kayak paddle blades of different design. *Sports Engineering*, **6**, 11-20.

Toussaint, H. M., Van den, B. C., & Beek, W. J. (2002). "Pumped-up propulsion" during front crawl swimming. *Medicine and Science in Sports and Exercise*, **34**, 314-319.

Figure captions

Figure 1

Overhead view of a single scull showing the forces occurring during the drive phase of the stroke, along with the oar shaft dimensions. The single scull is shown at two time points and the measured path of the centre of the oar blade is shown for a right handed oar (--) (Kleshnev, 1999).

Figure 2

Frontal view of the Big Blade (A) and Macon (B) oar blade designs is shown, along with the orientation of oar shaft attachment for each.

Figure 3

The movement of a right handed oar blade during the drive phase of the rowing stroke with the boat moving from left to right. The approximate directions of the lift and drag forces generated are indicated (adapted from Dreissigacker & Dreissigacker (2000)).

Figure 4

Plan (A) and side (B) views of the measurement system used to measure the normal and tangential oar blade forces, through the use of strain gauges A, B, G, H and V.

Figure 5

Plan view of the water flume showing the orientation of the oar blade. The direction of lift and drag forces are illustrated, along with the measured normal and tangential oar blade forces and the chord line of the blade.

Figure 6

Lift (---) and drag (—) coefficients are plotted against angle of attack for a flat plate.

Figure 7

Lift coefficients are shown for both C_{Lmax} (at 45 degrees) (■) and C_{Lmin} (at 135 degrees) (▲), along with drag coefficient for C_{Dmax} (at 90 degrees) (●) at a range of fluid velocities to determine the influence of Reynolds number.

Figure 8

Lift (●/○) and drag (■/□) coefficients are compared for the flat (—) and curved Big Blade (---). x at the top of the figure signifies significant differences between blade designs for drag coefficient and along the bottom of the figure for lift coefficient ($p < 0.01$).

Figure 9

Lift (●/○) and drag (■/□) coefficients are compared for the Big Blade (---) and Macon (—) oar blade designs. x at the top of the figure signifies significant differences between blade designs for drag coefficient and along the bottom of the figure for lift coefficient ($p < 0.01$).

Figures

<u>Figure 1.</u>

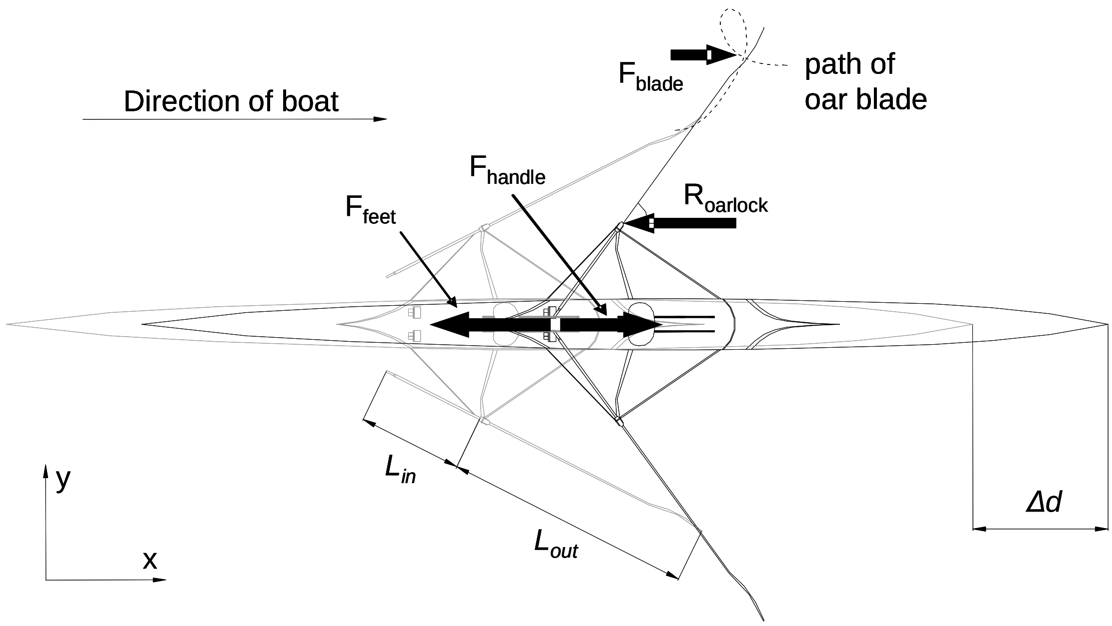

Figure 2.

A

B

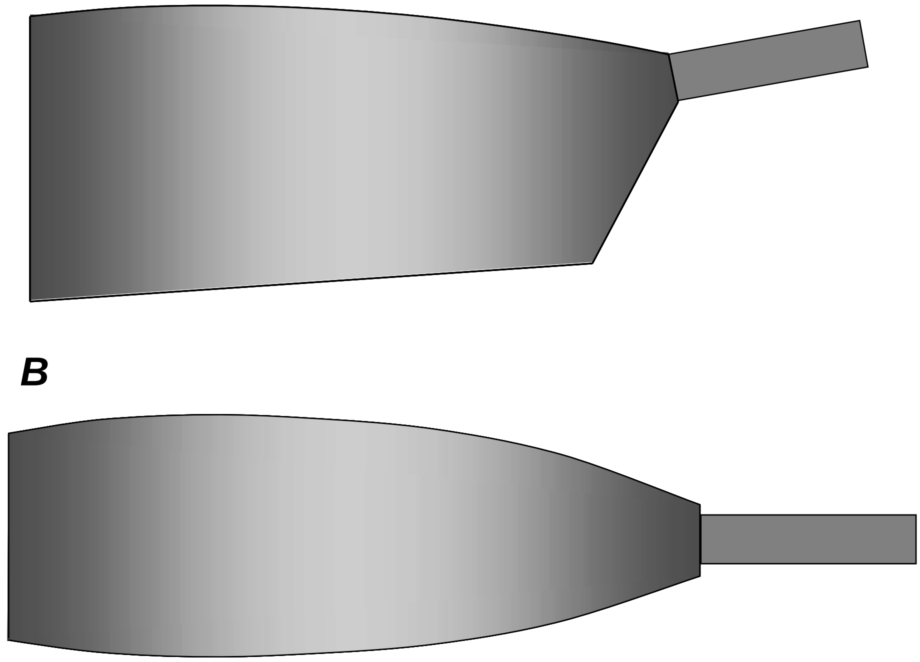

Figure 3.

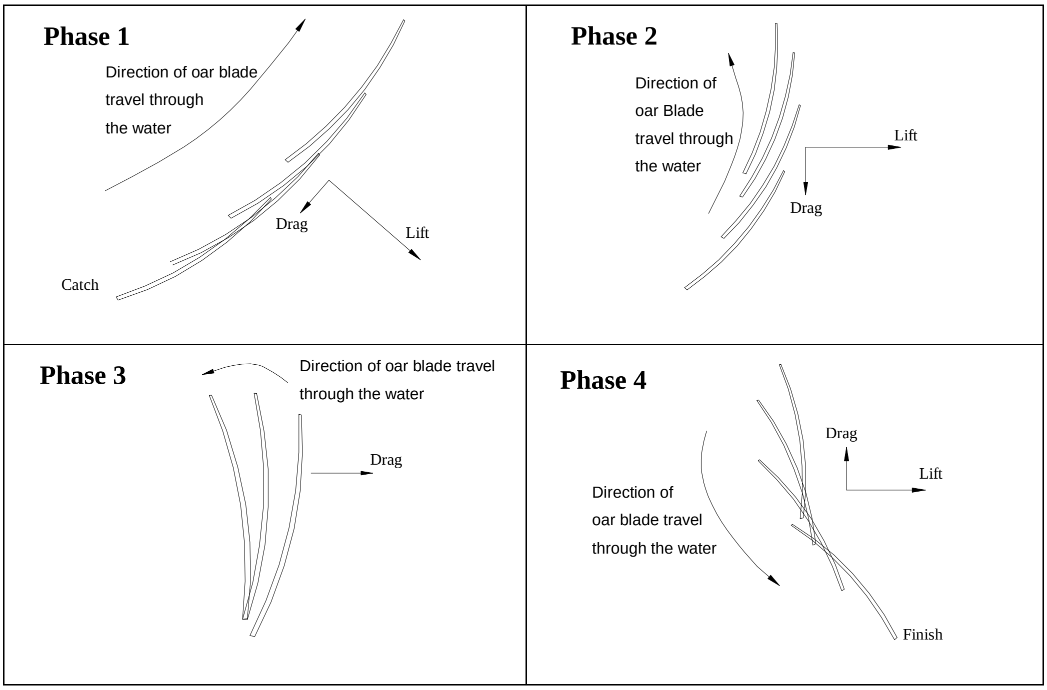

Phase 1
Direction of oar blade
travel through
the water
Drag
Lift
Catch
Phase 2
Direction of
oar Blade
travel through
the water
Lift
Drag
Phase 3
Direction of oar blade travel
through the water
Drag
Phase 4
Drag
Lift
Direction of
oar blade travel
through the water
Finish

Figure 4.

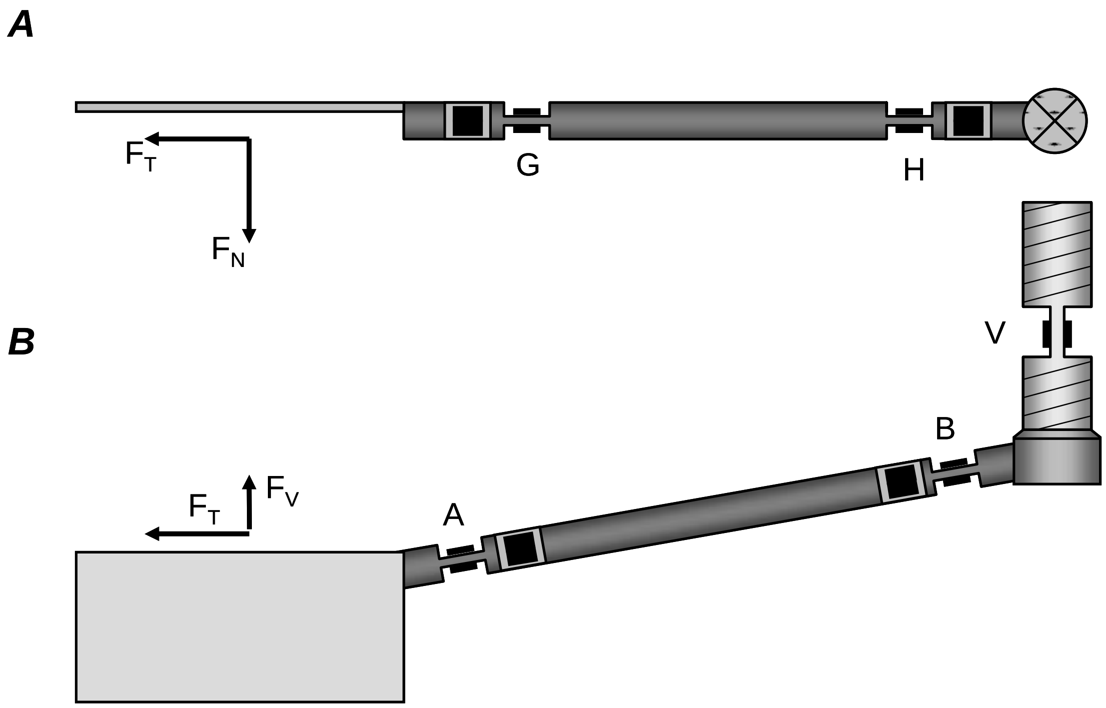

Figure 5.

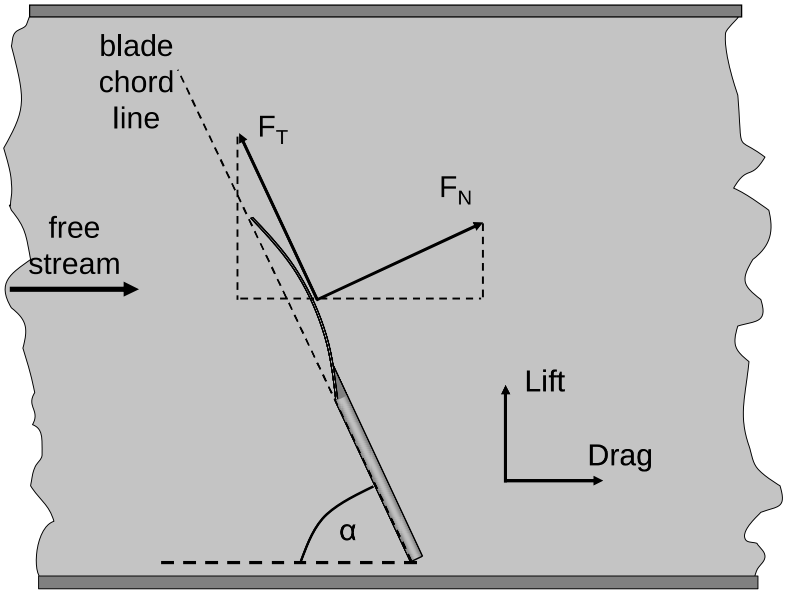

Figure 6.

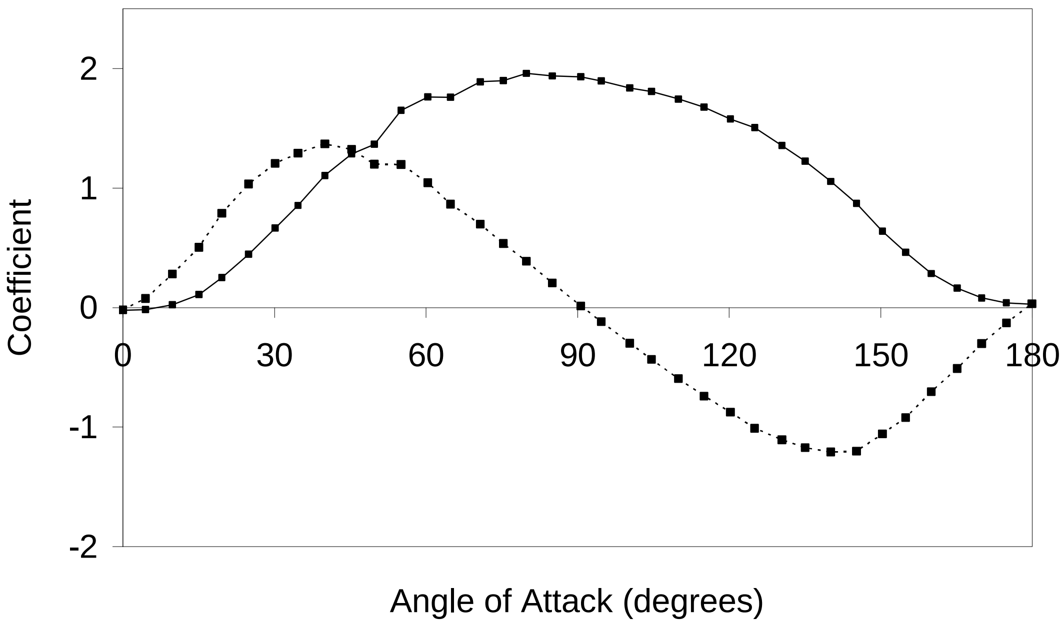

2
1
0
-1
-2
Coefficient
0
30
60
90
120
150
180
Angle of Attack (degrees)

Figure 7.

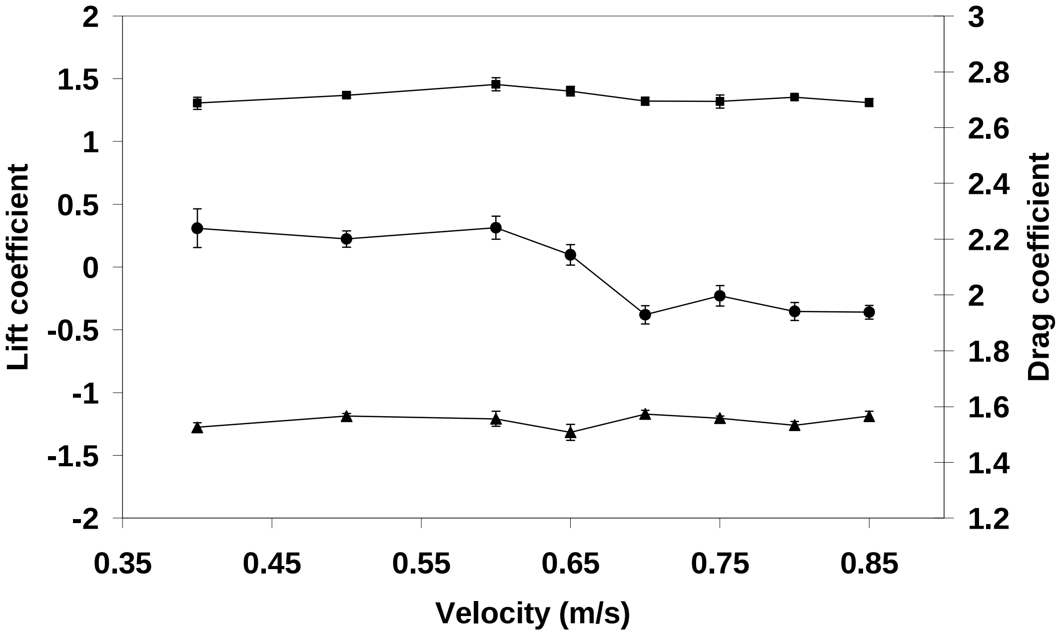

2
1.5
1
0.5
0
-0.5
-1
-1.5
-2
Lift coefficient
3
2.8
2.6
2.4
2.2
2
1.8
1.6
1.4
1.2
Drag coefficient
0.35
0.45
0.55
0.65
0.75
0.85
Velocity (m/s)

Figure 8.

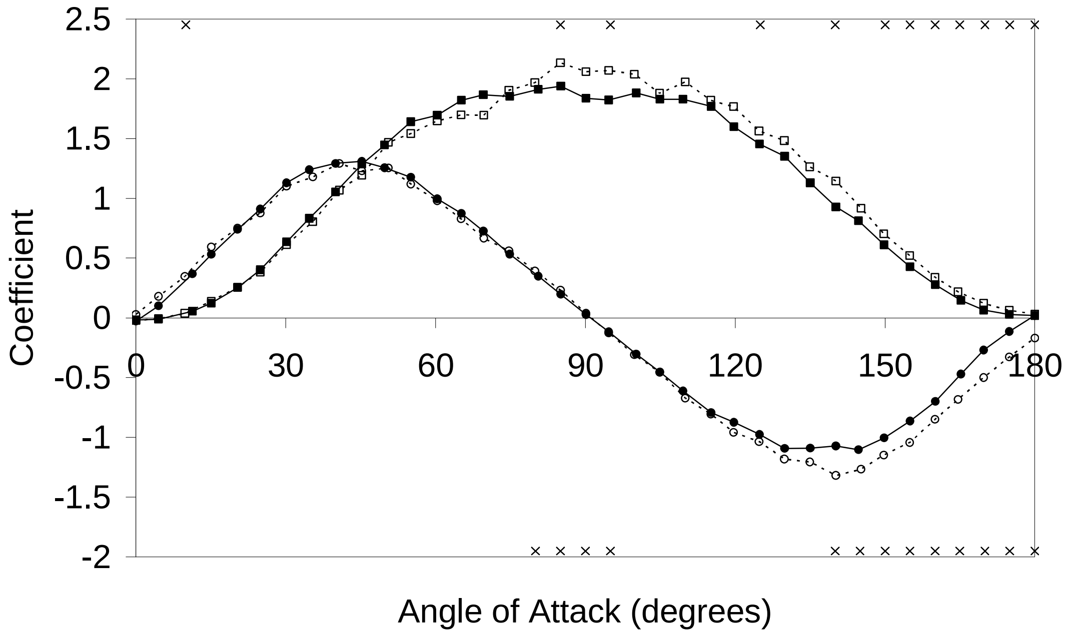
2.5
2
1.5
1
0.5
0
-0.5
-1
-1.5
-2
0
30
60
90
120
150
180
Coefficient
Angle of Attack (degrees)

Figure 9.

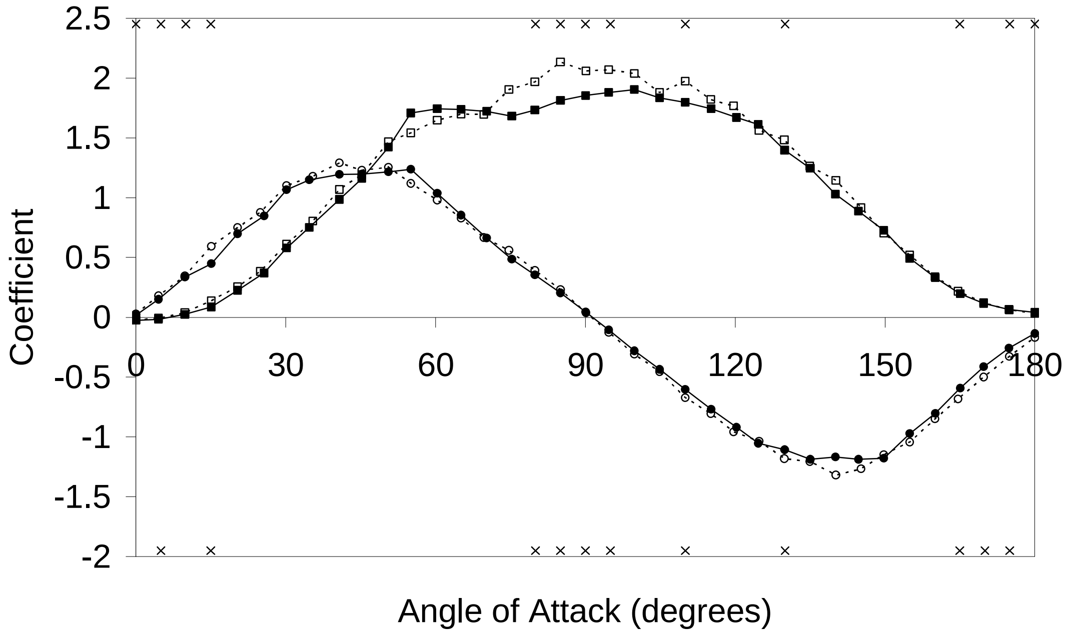

2.5
2
1.5
1
0.5
0
-0.5
-1
-1.5
-2
Coefficient
0
30
60
90
120
150
180
Angle of Attack (degrees)